

Crucial Role of *Drosophila* Neurexin in Proper Active Zone Apposition to Postsynaptic Densities, Synaptic Growth, and Synaptic Transmission

Jingjun Li,¹ James Ashley,² Vivian Budnik,^{2,3} and Manzoor A. Bhat^{1,3,*}

¹Curriculum in Neurobiology, Department of Cell and Molecular Physiology, UNC-Neuroscience Center, Neurodevelopmental Disorders Research Center, University of North Carolina School of Medicine, Chapel Hill, NC 27599-7545, USA

²Department of Neurobiology, University of Massachusetts Medical School, Worcester, MA 01605, USA

³These authors contributed equally to this work.

*Correspondence: manzoor_bhat@med.unc.edu

DOI 10.1016/j.neuron.2007.08.002

SUMMARY

Neurexins have been proposed to function as major mediators of the coordinated pre- and postsynaptic apposition. However, key evidence for this role in vivo has been lacking, particularly due to gene redundancy. Here, we have obtained null mutations in the single *Drosophila* *neurexin* gene (*dnrx*). *dnrx* loss of function prevents the normal proliferation of synaptic boutons at glutamatergic neuromuscular junctions, while *dnrx* gain of function in neurons has the opposite effect. DNRX mostly localizes to the active zone of presynaptic terminals. Conspicuously, *dnrx* null mutants display striking defects in synaptic ultrastructure, with the presence of detachments between pre- and postsynaptic membranes, abnormally long active zones, and increased number of T bars. These abnormalities result in corresponding alterations in synaptic transmission with reduced quantal content. Together, our results provide compelling evidence for an in vivo role of neurexins in the modulation of synaptic architecture and adhesive interactions between pre- and postsynaptic compartments.

INTRODUCTION

Synapse development and function form the basis of many neuronal processes, including formation and function of neural circuits, the ability to learn, and the ability to store and recall memories. Thus, elucidating the mechanisms by which synapses develop and are modified is a central question in neurobiology. Over the past few decades, a number of factors have been identified that play major roles in synapse morphogenesis and synaptic plasticity. Among these, *trans*-synaptic cell adhesion and signaling molecules that mediate the interactions

between pre- and postsynaptic membranes stand out. They are thought to mediate target recognition, induce pre- and postsynaptic specializations and their alignment during synaptogenesis, maintain the integrity of synapses, and regulate synaptic assembly and disassembly during synaptic development and remodeling (Garrow and El-Husseini, 2006; Scheiffele, 2003; Yamagata et al., 2003). In particular, neurexins and their postsynaptic binding partners the neuroligins are emerging as key synapse-organizing molecules.

Neurexins were first identified as primary receptors for α -latrotoxin, a neurotoxin that triggers massive neurotransmitter release (Ushkaryov et al., 1992). There are three *neurexin* genes in mammals, each of which has two promoters generating α - and β -neurexins. Neurexins are subject to extensive alternative splicing, generating a large number of variants, which may mediate target recognition and synaptic specificity (Missler and Sudhof, 1998; Rowen et al., 2002; Tabuchi and Sudhof, 2002). Recent studies on the functional significance of a small subset of neurexin splicing variants support this idea (Comolletti et al., 2006; Chih et al., 2006; Graf et al., 2006). The extracellular region of neurexins binds to neuroligins (Ichtchenko et al., 1995; Boucard et al., 2005) and dystroglycan (Sugita et al., 2001). Neuroligins are localized to postsynaptic densities (PSDs) (Song et al., 1999) and associated with neurotransmitter receptors by interaction with scaffolding proteins (Irie et al., 1997; Meyer et al., 2004). Intracellularly, neurexins interact with the synaptic vesicle protein synaptotagmin (Hata et al., 1993) and PDZ domain proteins CASK (Hata et al., 1996) and Mints (Biederer and Sudhof, 2000), which are linked to the synaptic vesicle exocytosis machinery (Atasoy et al., 2007; Ho et al., 2003). Thus, the *trans*-synaptic interaction between neurexin and neuroligin may bridge the synaptic cleft aligning the presynaptic neurotransmitter release machinery with postsynaptic densities. Important findings from cell culture studies indicate that neurexins and neuroligins could act bidirectionally to induce pre- and postsynaptic assembly, thus controlling synapse formation (Scheiffele et al., 2000; Graf et al., 2004; Dean et al., 2003; Nam and Chen, 2005; Chih et al., 2005; Prange et al., 2004; Levinson

et al., 2005; Fu et al., 2003). Interestingly, phenotypic analyses of α -neurexin triple-knockout mice suggest that α -neurexins are required for neurotransmitter release but are dispensable for synapse formation (Missler et al., 2003; Zhang et al., 2005). Thus, despite the expanding evidence indicating that neurexins may act as synaptic recognition and organizer molecules in synapse development and function, the complexity and redundancy of neurexin genes in mammals pose a tremendous difficulty in understanding their function in vivo.

A potential strategy to resolve these issues is to use simpler model systems, such as the fruit fly, to investigate the in vivo function of neurexins. Unfortunately, the first neurexin-related gene isolated in *Drosophila*, *neurexin IV* (*nrx IV*), is primarily expressed in epithelial and glial cells, where it is required for the organization and function of septate junctions (Baumgartner et al., 1996; Banerjee et al., 2006; Faivre-Sarrailh et al., 2004). *NRX IV* has an identical domain structure to contactin-associated protein 1 (Caspr1), a member of the Caspr family, which is distantly related to the neurexin family and mediates neuron-glia interactions (Bellen et al., 1998; Bhat et al., 2001; Peles et al., 1997; Poliak et al., 1999). A major breakthrough, however, came about upon the near completion of the *Drosophila* genome project (Adams et al., 2000), which led to the identification of a single gene with striking conservation with mammalian neurexins, resurrecting the initial idea of using the *Drosophila* system to understand neurexin function at synapses.

Here, we report the isolation of *Drosophila neurexin* (*dnrx*) null mutants and the characterization of its function during synapse development. Our results demonstrate that *dnrx* plays a critical role in the cytoarchitecture of synapses and during synapse development and function. These studies provide a better understanding of neurexin function in an intact organism and offer a strong basis for the interpretation of observations at mammalian central synapses.

RESULTS

DNRX Is the Single *Drosophila* Homolog of Vertebrate Neurexins

To identify a neurexin homolog in *Drosophila*, the rat neurexin 1 α cDNA sequence (Ushkaryov et al., 1992) was blasted against the *Drosophila* genomic and EST databases. We identified an EST (*LP03809*) with significant homology to the C-terminal sequences of vertebrate neurexins. This EST was subsequently used to screen a 0–20 hr old embryonic cDNA library to obtain a full-length *dnrx* cDNA (GenBank number *EF460788*). In contrast to the presence of three neurexin genes in mammals, our genome-wide search revealed only a single *neurexin* gene (*CG7050*) in *Drosophila* (also reported by Tabuchi and Sudhof, 2002; Zeng et al., 2007), which we named *Drosophila neurexin* (*dnrx*). The DNRX protein has an identical domain structural organization to mammalian

α -neurexins (Figure 1A). The large extracellular region consists of an N-terminal signal peptide and three LamG-EGF-LamG repeats. Although the cytoplasmic region of DNRX is longer than the mammalian counterparts, the PDZ binding motif at the C terminus is highly conserved (Figure 1C). Overall, DNRX is 36%–37% identical to human α -neurexins and shares high amino acid sequence identity with mammalian neurexins within each individual protein domain (Figure 1A).

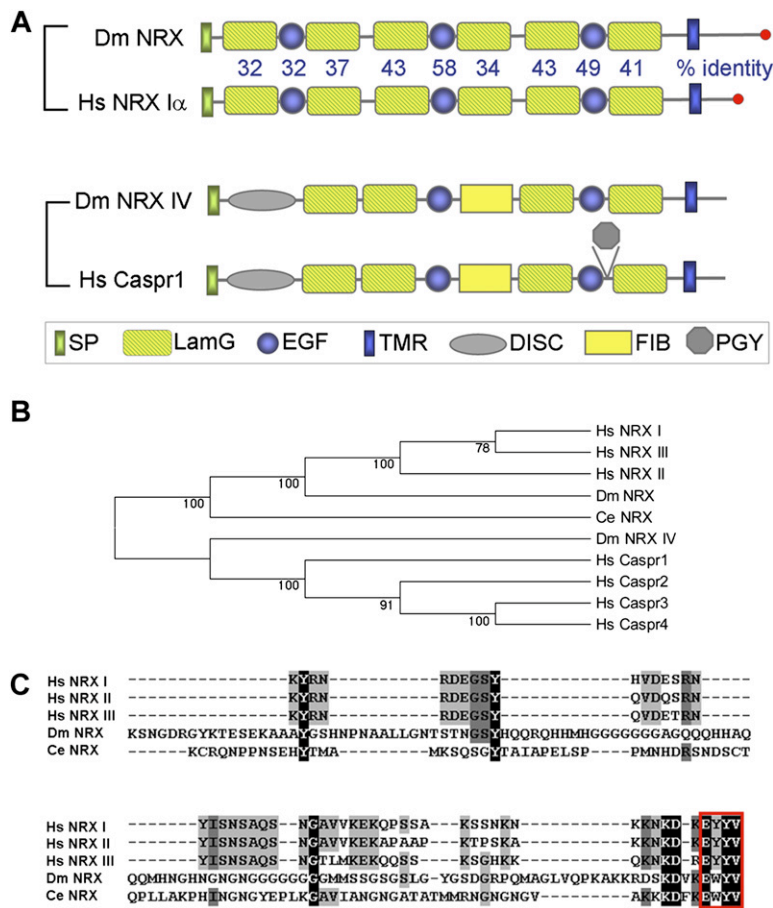
Previously, the *Drosophila* gene *nrx IV* was identified and proposed to belong to the neurexin family (Baumgartner et al., 1996). However, the domain arrangement of *NRX IV* differs from that of classical neurexins (Figure 1A). Furthermore, our phylogenetic analysis shows that DNRX is the closest homolog of vertebrate neurexins, whereas *NRX IV* is only distantly related to neurexins (Figure 1B).

DNRX Is Expressed in Central Neurons and Concentrated at Active Zones of Glutamatergic Neuromuscular Junctions

To determine where DNRX function might be required during development, we performed in situ hybridization to examine *dnrx* expression during embryonic stages. In situ hybridization using two independent RNA probes revealed that *dnrx* expression was enriched in central neurons (Figures 2A and 2B) but undetectable in muscle cells (Figure 2C). *dnrx* mRNA first appeared in subsets of central neurons at late stage 14, when axon pathfinding is nearly complete and the differentiation of presynaptic terminals is about to begin. This expression reached its highest levels at stages 16 and 17, when a larger number of neurons in the brain and ventral nerve cord expressed *dnrx* at elevated levels (Figures 2A and 2B). Low levels of *dnrx* expression could also be detected in small subsets of peripheral nervous system neurons.

The subcellular localization of DNRX was determined by immunocytochemical analysis using an affinity-purified polyclonal antibody generated against the cytoplasmic region of DNRX. In embryos, DNRX was concentrated in neuropil regions of the brain and ventral nerve cord, axon tracts of the ventral nerve cord, and motor axons (Figures 2D and 2E). The immunoreactivity was absent in homozygous embryos of *Df(3R)5C1*, which uncovers the *dnrx* gene, demonstrating the specificity of the DNRX antibody (Figure 2F). A similar DNRX distribution was observed in third-instar larvae (data not shown). In addition, DNRX was present at the glutamatergic type I boutons of the larval body wall muscles. This was confirmed by double staining with an antibody against the scaffolding protein discs-large (DLG) (Figures 2G–G''), which labels type I boutons, but not other bouton types (Figure 2G'; Lahey et al., 1994).

Confocal microscopy analysis revealed that within synaptic boutons DNRX immunoreactivity did not have a uniform distribution, but displayed discontinuous patches (Figures 2G–2K). To define the precise subcellular localization of DNRX in these patches, we used a number of synaptic markers. A presynaptic marker, bruchpilot

**Figure 1. Molecular Analysis of DNRX**

(A) Domain structure of DNRX, neurexin I α , neurexin IV, and Caspr1. The percent amino acid identity between DNRX and human neurexin I α in specific domains is indicated. SP, signal peptide; LamG, laminin G domain; EGF, EGF repeat; DISC, discoidin-like domain; FIB, a region similar to fibrinogen; PGY, PGY repeat; TMR, transmembrane region; Dm, *Drosophila melanogaster*; Hs, *Homo sapiens*; Ce, *C. elegans*.

(B) Phylogenetic analysis of human, *Drosophila*, and *C. elegans* neurexins, *Drosophila* neurexin IV, and human Caspr proteins using the neighbor-joining method (Mega 3.1; Kumar et al., 2004). DNRX and NRX IV belong to the neurexin and Caspr subfamily, respectively. Numbers along each branch are the bootstrap confidence value.

(C) Multiple sequence alignment (ClustalW) of cytoplasmic sequences of *Drosophila*, *C. elegans*, and human neurexins. The PDZ binding motif at the C termini of neurexins is boxed.

(BRP; Wagh et al., 2006; Kittel et al., 2006), is thought to label at least one component of the active zone, the T bar (see below). Bright DNRX patches were juxtaposed and slightly overlapped with almost every BRP spot, as revealed by examining the labels in thin consecutive confocal slices (Figures 2H–2H'', arrows and insets). In addition, DNRX appeared to surround BRP immunoreactivity. Notably, the postsynaptic density (PSD) marker *Drosophila* p21-activated kinase (PAK; Sone et al., 2000) also appeared juxtaposed to DNRX patches, but in contrast to BRP, minimal overlap between the labels was observed (Figures 2I–2I'', arrows and insets).

We next double labeled NMJ preparation with DNRX and the so-called periaxial zone markers, such as the SH3 adaptor protein nervous wreck (NWK) (Coyle et al., 2004) and the cell adhesion molecule fasciclin II (FASII) (Sone et al., 2000). In general, DNRX showed no overlap with NWK, although occasionally colocalization between less intense DNRX regions and NWK immunoreactive regions was observed (Figure 2J). In the case of FASII, there are significant regions of nonoverlap, with some regions displaying partial overlap (Figure 2K). Thus, DNRX appears to be concentrated at active zones but also extends into periaxial zones.

Genetic Analysis of *dnrx*

To determine the role of DNRX in synaptic development and function, we generated *dnrx* null mutants. The *dnrx* gene is predicted to comprise 13 exons and 12 introns, spanning ~13.4 kb. To disrupt the *dnrx* locus, we carried out an excision screen with a *P* element (*XPd08766*) located ~200 base pairs upstream of *dnrx*, which led to the isolation of two *dnrx* mutant alleles, *dnrx*²⁷³ and *dnrx*²⁴¹ (Figure 3A). The break points of the deletions were molecularly determined by PCR and sequence analysis. The *dnrx*²⁷³ allele had an ~8 kb deletion within the *dnrx* locus, which removed most of the coding sequence for the extracellular region of DNRX, from the start codon to the fourth LamG domain. *dnrx*²⁴¹ uncovered the entire *dnrx* gene and the upstream region of an adjacent transcription unit (Figure 3A). Western blot analysis with the DNRX C terminus specific antibody showed that an ~200 kDa DNRX band in wild-type was absent in *dnrx*²⁷³/*Df(3R)5C1*, and there was no detectable truncated protein in *dnrx* mutants (Figure 3B). Immunostaining with this antibody also showed no detectable protein in homozygous mutant embryos (data not shown) and NMJs (Figures 3C–3C') from both *dnrx* alleles, confirming that *dnrx*²⁷³ and *dnrx*²⁴¹ are null alleles. In this study, the

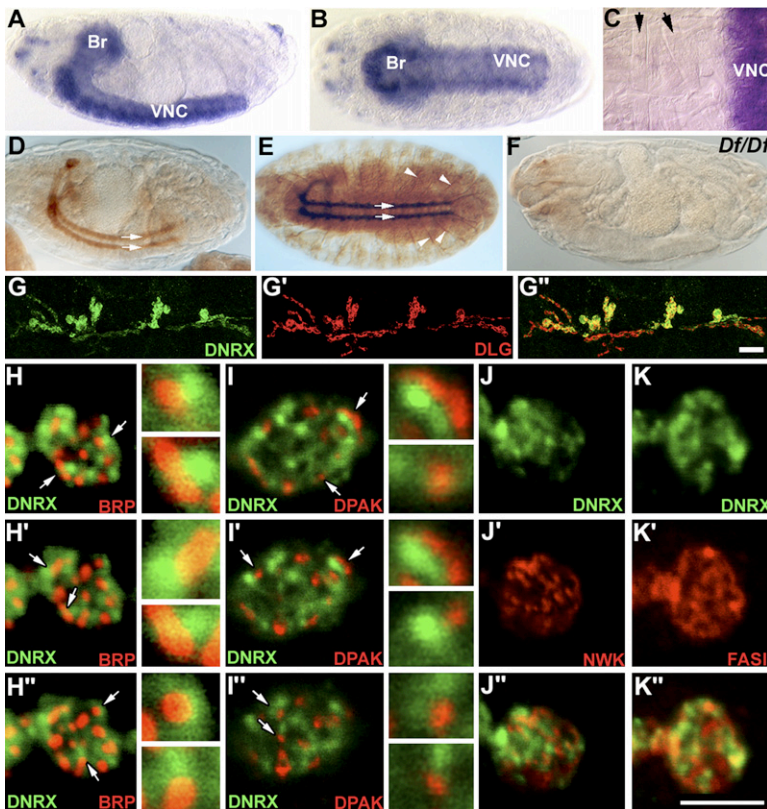


Figure 2. DNRX Is Expressed in Central Neurons and Concentrated at Active Zones of Glutamatergic NMJs

(A–C) In situ hybridization analysis of *dnrx* expression in wild-type embryos. (A) Lateral and (B) ventral view of *dnrx* mRNA distribution in the brain (Br) and ventral nerve cord (VNC) of a stage 17 whole-mount embryo. (C) Higher magnification of a dissected embryo showing that *dnrx* mRNA is enriched in central neurons but undetectable in muscle cells (arrows).

(D and E) Lateral and ventral view of wild-type embryos stained with anti-DNRX antibody, showing that DNRX is localized in the CNS neuropil and axonal tracts (arrows) and motor axons (E, arrowheads).

(F) A *Df(3R)5C1* homozygous embryo stained with anti-DNRX, showing the specificity of antibody.

(G–G') Double staining of wide-type third-instar larval NMJ 6/7 with anti-DNRX (green) and anti-DLG (red), which labels glutamatergic type I boutons. The merged DNRX and DLG image shows that DNRX is located at type I boutons.

(H–K'') Confocal images of synaptic boutons double labeled with anti-DNRX (green) and synaptic markers (red), showing that DNRX is concentrated at active zones but also extends into periaxial zones.

(H'–I'') Three consecutive single confocal slices from NMJs labeled with (H–H'') anti-DNRX and anti-BRP, showing that bright DNRX spots are juxtaposed and slightly colocalized with BRP

spots (given that DNRX spots were associated to one side of BRP spots, such juxtaposition could not be seen in every slice, but could be verified in a sequence of single slices), and (I–I'') anti-DNRX and anti-DPAK, showing that DPAK and DNRX largely do not colocalize. Columns to the right side of (H)–(I'') are high-magnification views of BRP–DNRX or DPAK–DNRX spots indicated in the low-magnification panels by arrows.

(J–J'') Single confocal scan of synaptic boutons double stained for DNRX and NWK, which localizes to the periaxial zone of presynaptic terminals, shows that DNRX and NWK localize to distinct areas and do not display any significant overlap.

(K–K'') Single confocal scan of synaptic boutons double stained for DNRX and FAS II, a cell adhesion molecule defines the periaxial zone of pre- and postsynaptic membrane, shows that most of DNRX staining regions do not overlap with that of FAS II.

Scale bars, 15 μ m (G''), 5 μ m (K'').

following allelic combinations were used for phenotypic analysis: *dnrx*²⁷³/*Df(3R)5C1*, *dnrx*²⁷³/*dnrx*²⁷³, and/or *dnrx*²⁷³/*dnrx*²⁴¹. A precise excision of the *P* element and a wild-type strain were used as controls.

***dnrx* Mutants Display Decreased Locomotor Activity and Abnormal NMJs**

α -neurexin triple-knockout mice and most double-knockout mutants die prematurely due to respiratory problems (Missler et al., 2003; Zhang et al., 2005). In contrast, 10% of the *dnrx*²⁷³/*Df(3R)5C1* progeny died at pupal stages while the remaining progeny survived to adulthood and were fertile. This partial lethality was rescued by expressing a *dnrx* full-length cDNA in neurons using the *C380-Gal4* driver (Budnik et al., 1996). *dnrx* mutants exhibited severely impaired behavior in larval stages, being uncoordinated and sluggish. Locomotor activity was reduced in all *dnrx* mutants, including the two *dnrx* alleles over deficiency and in allelic combinations. For the *dnrx*²⁷³/*Df(3R)5C1* line, this phenotype was quantified in

a larval locomotor assay. In this assay, the number of grids on a horizontal agar surface entered by individual third-instar wandering larvae within a 30 s time window over a test period of 180 s was counted. While control animals passed about five grids on average, *dnrx*²⁷³/*Df(3R)5C1* mutants entered less than two grids (Figure 3D). This phenotype was completely rescued by expressing DNRX in neurons using the *C380-Gal4* driver (Figure 3D). Thus, decreased locomotor activity is due to *dnrx* loss-of-function in neurons.

Given that DNRX is localized at larval NMJs, we reasoned that abnormal development and function of NMJs might be responsible for the behavioral deficits. Compared to controls (Figures 4A and 4E), *dnrx* mutants (Figure 4B, 4C, 4F, and 4G) had shortened axon branches with fewer boutons. In addition, mutant NMJ branches often contained long intervening axon stretches devoid of synaptic boutons. Further quantification revealed that *dnrx* mutants had a 40%–60% decrease in bouton number (Figures 4I and 4J). As with the behavioral

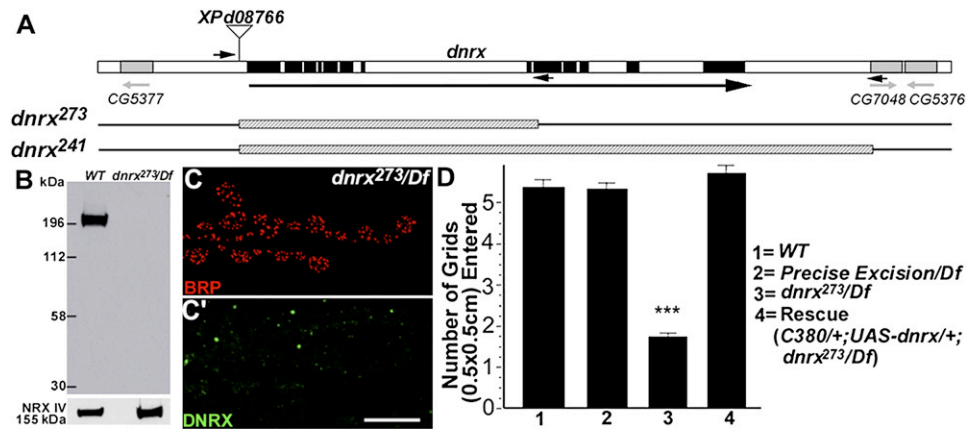


Figure 3. Generation and Characterization of *dnrx* Mutants

(A) Genomic structure of *dnrx* with the intron-exon organization. Exons are indicated by black boxes and introns by open boxes. The adjacent genes and directions of their transcription are denoted by gray boxes and arrows, respectively. The *P* element *XPd08766* is inserted ~200 bp upstream of *dnrx*. *dnrx* alleles (*dnrx²⁷³* and *dnrx²⁴¹*) with their deleted regions indicated by hatched boxes were generated by imprecise excisions of *XPd08766*. The primers used for PCR and sequencing to define the break points of deletions are indicated by black arrows.

(B) Western blot of adult head membrane extracts of wild-type and *dnrx²⁷³/Df* flies probed with anti-DNRX (upper panel) and reprobed with anti-NRX IV (lower panel). The ~200 kDa DNRX band is absent in *dnrx²⁷³/Df* mutants. NRX IV is the loading control.

(C–C') Double staining of *dnrx²⁷³/Df* mutant NMJ with anti-BRP (red) and anti-DNRX (green), showing that DNRX immunoreactivity is absent from synaptic boutons (C') where only BRP immunoreactivity is detected (C). Scale bar, 15 μ m.

(D) Quantification of locomotor activity of wall-wandering third-instar larvae. The *precise excision/Df* performed as well as wild-type, whereas *dnrx²⁷³/Df* displayed significantly reduced locomotor activity (***) ($p < 0.0001$). This phenotype was completely rescued with neuronal expression of a *dnrx* full-length cDNA (*C380/+; UAS-dnrx/+; dnrx²⁷³/Df*). For all genotypes, $n = 20$. Data are mean \pm SEM.

abnormalities, the reduced bouton number was fully rescued by expression of the *UAS-dnrx* transgene in neurons (Figures 4D, 4H, 4I, and 4J). Taken together, these results suggest that DNRX is required for proper proliferation of synaptic boutons during larval development, which is necessary for coordinated matching of pre- and postsynaptic compartments during this period of intense growth (Griffith and Budnik, 2006).

In addition to synaptic regions, DNRX is localized to axons as well. Therefore, we also investigated whether axon guidance and pathfinding were altered in *dnrx* mutants. The specificity of axon pathfinding was examined by immunostaining with BP102 and FASII antibodies, which stain all CNS axons and both a subset of CNS axonal fascicles and peripheral motor axons, respectively. No apparent defects were observed in both CNS axonal pathways and muscle innervation patterns in *dnrx* mutants (data not shown).

Neuronal Expression of DNRX Promotes Proliferation of Synaptic Boutons

Studies in cell culture have indicated that neurexins and their postsynaptic binding partners, the neuroligins, induce synapse formation (Graf et al., 2004; Chih et al., 2005; Scheiffele et al., 2000; Dean et al., 2003). Therefore, we asked whether *dnrx* could similarly induce the formation of new synaptic boutons. Expression of a full-length *dnrx* transgene in wild-type background, using two different neuron-specific Gal4 drivers, the pan-neural driver *elav* (Lin and Goodman, 1994) and neural driver *C380*,

significantly enhanced the formation of synaptic boutons (Figure 5C, compare with Figures 5A and 5B). Increasing *dnrx* gene dosage in all neurons by one copy resulted in over a 30% increase in the number of synaptic boutons, while increasing it by two copies resulted in more than 40% enhancement (Figure 5D). A similar trend was observed by using *C380-Gal4* (Figure 5D).

Recent studies on murine central synapses suggest that postsynaptic neurexins affect glutamate receptor function and may also inhibit neuroligin function via cis interaction with neuroligins on the postsynaptic membrane (Kattenstroth et al., 2004; Taniguchi et al., 2007). To explore the potential functional relevance of DNRX in the postsynaptic compartment at NMJs, we examined whether muscle expression of DNRX had any effect on synaptic growth. Compared to genetic background matched controls, expression of either one or two copies of a *dnrx* transgene in muscle cells, using the *C57 Gal4* driver (Budnik et al., 1996), did not result in any significant change in bouton number (Figure 5E). Taken together, the DNRX loss- and gain-of-function analyses demonstrate that DNRX is necessary to promote the proliferation of synaptic boutons and further suggest that for this function DNRX is required in the pre- but not in the postsynaptic compartment.

DNRX Is Required for Pre- and Postsynaptic Differentiation

We also explored whether the expression and localization of synaptic proteins were affected in *dnrx* mutants. The abundance and localization of periaxonal zone proteins,

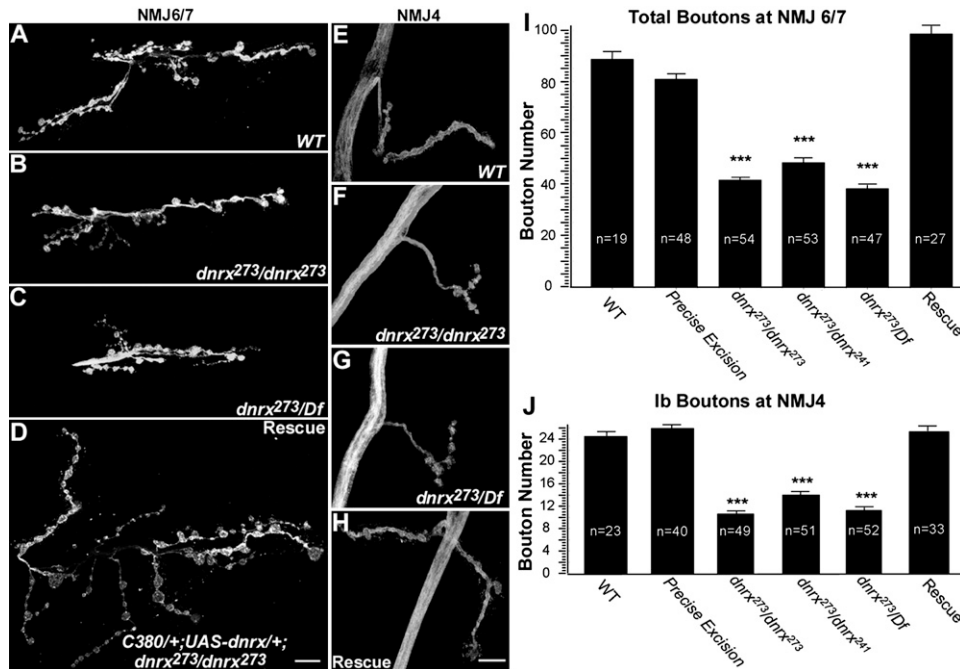


Figure 4. DNRX Loss-of-Function Leads to Reduced Synaptic Bouton Number at Larval NMJs

(A–H) NMJ morphology at muscle 6/7 (A–D) and muscle 4 (E–H) of larval abdominal segment 3 labeled with anti-HRP. Compared to wild-type (A and E), *dnrx* null mutants *dnrx²⁷³/dnrx²⁷³* (B and F) and *dnrx²⁷³/Df* (C and G) have less NMJ expansion, shorter axonal branches, and fewer boutons. A rescue line with neuronal expression of *UAS-dnrx* cDNA in *dnrx²⁷³/dnrx²⁷³* background appears to restore NMJ morphology (D and H). Scale bars, 15 μ m.

(I and J) Quantification of total bouton number at NMJ 6/7 (I) and type Ib bouton number at NMJ4 (J). Both quantifications show that *dnrx* mutants *dnrx²⁷³/dnrx²⁷³*, *dnrx²⁷³/dnrx²⁴¹*, and *dnrx²⁷³/Df3R(5C1)* have a significant decrease in average bouton number when compared to wild-type and precise excision homozygotes. The reduced bouton number is completely rescued by restoring DNRX expression in neurons (rescue: *C380/+; UAS-dnrx/+; dnrx²⁷³/dnrx²⁷³*). ****p* < 0.001; data are mean \pm SEM.

such as the cell adhesion molecule FASII, the cytoskeleton adaptor protein NWK, and the endocytotic protein Dap160 (Roos and Kelly, 1999; Koh et al., 2004; Marie et al., 2004), appeared unchanged in *dnrx* mutants (see Figure S1 in the Supplemental Data available with this article online). Several other synaptic proteins, including the scaffolding PDZ protein DLG and the microtubule-binding protein Futsch (Roos et al., 2000; Hummel et al., 2000), also appeared unaffected in *dnrx* mutants (data not shown). However, profound abnormalities in the distribution of synaptic vesicle and active zone proteins, as well as glutamate receptor (GluR) clusters, were observed in *dnrx* mutant NMJs.

In wild-type, synaptotagmin (Synt), a synaptic vesicle protein, is efficiently transported to presynaptic terminals; therefore, it is seldom observed within motor axons (Figures 6A–6A' and 6D; Littleton et al., 1993). In *dnrx* mutants, however, intense punctate Synt staining was often observed in motor axons (Figures 6B–6B' and 6D). Similarly, the active zone protein BRP, which is rarely seen in wild-type axons, was also mislocalized to mutant axons (Figures 6C–6C'). Notably, BRP immunoreactivity colocalized with Synt at these accumulations along the motor axons, suggesting that DNRX is

involved in the proper recruitment, localization, or transport of key synaptic components during presynaptic differentiation.

At mammalian synapses it has been hypothesized that neuroligins are required for the alignment of pre- and postsynaptic compartments (Graf et al., 2004; Yamagata et al., 2003). Therefore, we next examined whether pre- and postsynaptic apposition was affected in *dnrx* mutants by double labeling synaptic boutons with the presynaptic active zone marker BRP and the PSD markers DPAK and GluRIII (Marrus et al., 2004). No gross defects in pre- and postsynaptic alignment was observed (Figures 6E'', 6F'', 6G'', and 6H''). DPAK and GluRIII clusters were exactly juxtaposed to active zones in *dnrx* mutants. However, the size of DPAK and GluRIII clusters was markedly enlarged in mutant boutons (Figures 6F' and 6H' [compare with Figures 6E' and 6G']). Enlargement of GluRIII clusters was also observed, while the GluRIII intensity in boutons was not statistically different between mutant and wild-type (Figure S2). Taken together, these results suggest that although the juxtaposition of pre- and postsynaptic components is not altered at least at the light-microscopic level, the distribution of PSD proteins is affected in *dnrx* mutants.

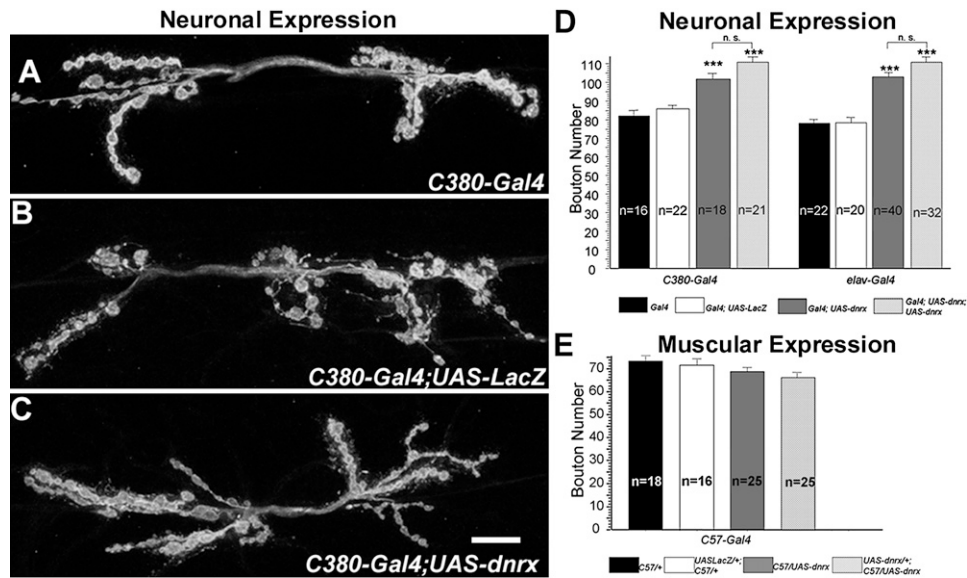


Figure 5. Neuronal but Not Muscular Overexpression of DNRX Promotes Proliferation of Synaptic Boutons

(A–C) NMJ morphology at muscle 6/7 in animals with DNRX overexpression in neurons. Compared with control animals (A) that lack *dnrx* transgene (*C380-Gal4*) or (B) that overexpress an unrelated gene (*C380-Gal4; UAS-lacZ*) in neurons, (C) animals with DNRX overexpression in neurons (*C380-Gal4; UAS-dnrx*) have more branching and boutons. Scale bar, 15 μ m.

(D) Quantification of bouton number shows that animals overexpressing either one- (*Gal4; UAS-dnrx*) or two-copy (*Gal4; UAS-dnrx; UAS-dnrx*) *dnrx* transgene driven by either neuron (*C-380*) or pan-neuron (*elav*) Gal4 drivers have a significant increase in average bouton number when compared to control animals that lack a *dnrx* transgene (*Gal4*) or that express an unrelated gene (*Gal4; UAS-LacZ*). *** $p < 0.001$, Data are mean \pm SEM.

(E) Quantification of bouton number shows that there is no significant change in average bouton number between animals that express *dnrx* transgene in muscles driven by C57 Gal4 and control animals. Data are mean \pm SEM.

Active Zones and PSDs Are Altered in *dnrx* Mutants

To determine the significance of the light-microscopic phenotypes described above, we carried out ultrastructural and functional analyses of NMJs in *dnrx* mutants. For the ultrastructural studies, *dnrx* mutant and control NMJs were serially sectioned and subjected to a morphometric analysis. *dnrx* mutants had striking structural abnormalities in active zones and PSDs of type Ib boutons. Wild-type boutons are characterized by the presynaptic compartment containing synaptic vesicles, mitochondria, and endosomes (b in Figure 7A). At the presynaptic membrane, active zones are composed of regulatory electron-dense structures, the T bars (arrow in Figures 7A and 7C) containing BRP/CAST (Kittel et al., 2006; Wagh et al., 2006), and the presynaptic densities (PRDs), the likely sites for synaptic vesicle fusion (Figure 7C). The PRDs are exactly juxtaposed to PSDs (between arrowheads in Figures 7C and 7E), which contain GluRs in high-density clusters (Prokop and Meinertzhagen, 2006). Separating both membranes is the synaptic cleft, which has a uniform size and is filled with material that differs in electron density and structure from the rest of the bouton extracellular space (Figures 7A, 7C, and 7E).

Several features of the active zones and PSDs were altered in *dnrx/Df* mutants. PRDs and apposed PSDs were over 60% longer in the mutants compared to

controls (Figures 7D and 7G). This is in agreement with the light-microscopic studies showing that DPAK and GluR clusters were increased in size in *dnrx* mutants. In addition, the number of T bars per bouton was increased by more than 2-fold (Figures 7B and 7G). Most strikingly, the PRD showed signs of detachment from the PSD, a phenotype that is rarely seen in wild-type (Figures 7D, 7F, and 7G). In these *dnrx* mutant synapses, PRDs showed bleb-like invaginations at several points, and at these sites the typical electron density of PRDs was lost (Figure 7F). The material at the synaptic cleft also appeared altered, but no defects were observed at the corresponding sites of the PSDs (Figure 7F). Thus, in *dnrx* mutants, synapses within synaptic boutons are dramatically altered, showing sites of presynaptic membrane detachment, abnormally long active zones, and increased number of T bars. The increase in the number of T bars and the aberrant detachment of PRD were completely or almost completely rescued by expressing a *dnrx* transgene in the mutant background, respectively (Figure 7G). However, the increased length of the active zones was only partially rescued by the transgene, suggesting that this phenotype might be highly sensitive to DNRX dosage. Our ultrastructural analysis of *dnrx* mutant synaptic boutons provides direct in vivo evidence supporting the model that neurexins are involved in adhesion between the pre- and the postsynaptic cells.

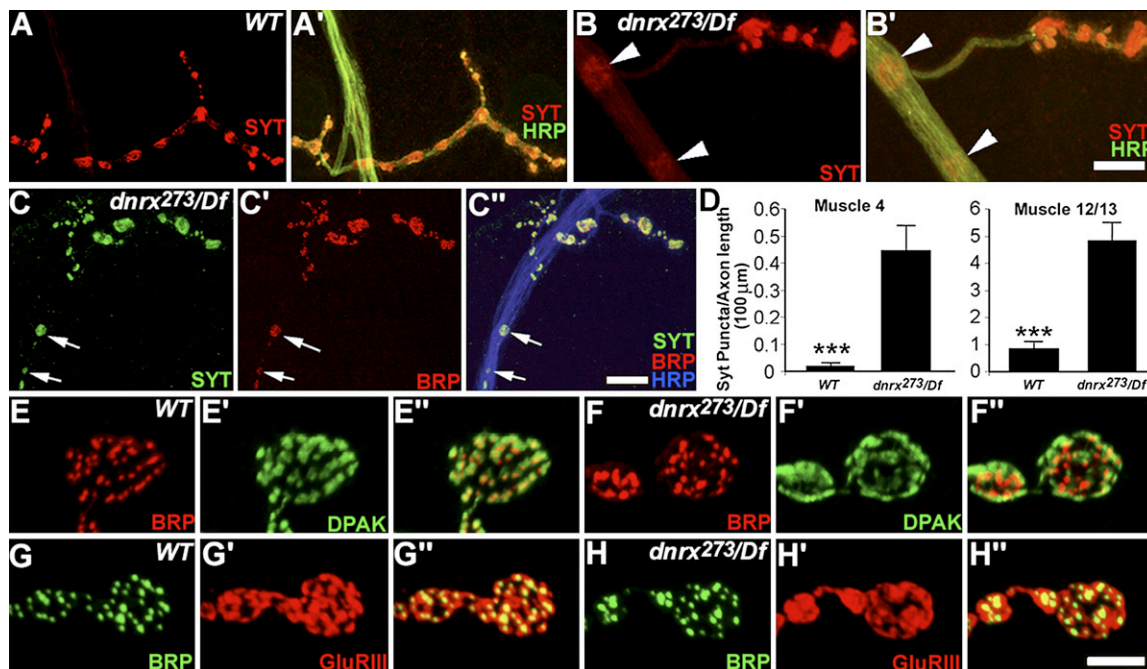


Figure 6. Distribution of Pre- and Postsynaptic Proteins Is Altered in *dnrx* Mutants

(A–B') NMJ 4 stained with anti-Syt (red) and anti-HRP (green) in wild-type (A and A') and *dnrx* mutant (B and B'). *dnrx* mutants display accumulation of Syt staining puncta in motor axons (B and B', arrowheads).

(C–C'') NMJ 4 of *dnrx* mutant stained with anti-Syt (green), anti-BRP (red), and anti-HRP (blue), showing colocalization of Syt and BRP staining (arrows) in accumulated puncta along the axon.

(D) Quantification of Syt-puncta observed in axons innervating muscle 4 and muscle 12/13 shows that *dnrx* mutants have significantly increased Syt accumulation per unit axon length. $n > 76$; *** $p < 0.001$. Data are mean \pm SEM.

(E–F'') Synaptic boutons of wild-type (E–E'') and *dnrx* mutant (F–F'') double stained for BRP (red) and DPAK (green), which labels the pre- and postsynaptic active zone, respectively. The pre- and postsynaptic alignment appears grossly unaffected in *dnrx* mutants. However, the distribution of DPAK within synaptic boutons is increased in *dnrx* mutant.

(G–H'') Synaptic boutons of wild-type (G–G'') and *dnrx* mutant (H–H'') double stained for BRP (green) and GluRIII (red). The apposition of GluRIII and BRP staining appears normal in *dnrx* mutants. However, the distribution of GluRIII cluster is enlarged in *dnrx* mutants.

Scale bar, 15 μ m (B' and C''), 5 μ m (H).

***dnrx* Mutants Have Defects in Synaptic Transmission that Correlate with the Alterations in Synapse Ultrastructure**

To assess the functional consequences of the reduced bouton number, the enlarged GluR clusters, the increase in the size of active zones and PSDs, and the abnormal detachments of PRDs, we carried out an electrophysiological analysis of NMJs (Figure 8). For these experiments, the amplitude of spontaneous miniature excitatory potentials (mEJPs) was measured by intracellular recordings of muscles at low Ca^{2+} concentrations. In addition, the amplitude and kinetics of evoked excitatory potentials (EJPs) were measured by stimulating the segmental nerve containing the motor axons. Several defects were observed in *dnrx* mutants. Evoked synaptic transmission was reduced, as manifested by a small but significant decrease in the amplitude of EJPs. In addition, the frequency and amplitude of mEJPs was dramatically increased, suggesting both a pre- and a postsynaptic defect. Overall, quantal content was reduced, indicating defective synaptic transmission. The defect in EJP amplitude was com-

pletely rescued by expressing a *dnrx* transgene in neurons using *C380-Gal4* or ubiquitously using *T80-Gal4*. However, no rescue of the mEJP amplitude or frequency was observed, consistent with the ultrastructural studies, in which the size of the active zones and PSDs was only partially rescued by the *dnrx* transgene. This partial rescue is not surprising given that neuronal expression of a *dnrx* transgene in wild-type background also has deleterious effects on quantal content. It is notable that the functional abnormalities were observed in homozygous *dnrx*²⁷³ mutants, *dnrx*²⁷³/*dnrx*²⁴¹ combinations, as well as *dnrx* over a deficiency chromosome. Thus, they are unlikely to result from any genetic background effects.

Mutations in *dnrx* Have Abnormal Calcium Sensitivity without Altering the Distribution of Presynaptic Calcium Channels

Studies in mammals have suggested that neuroligins are involved in coupling Ca^{2+} channels to synaptic vesicle exocytosis apparatus (Missler et al., 2003). Therefore, we next examined whether the Ca^{2+} sensitivity of neurotransmitter

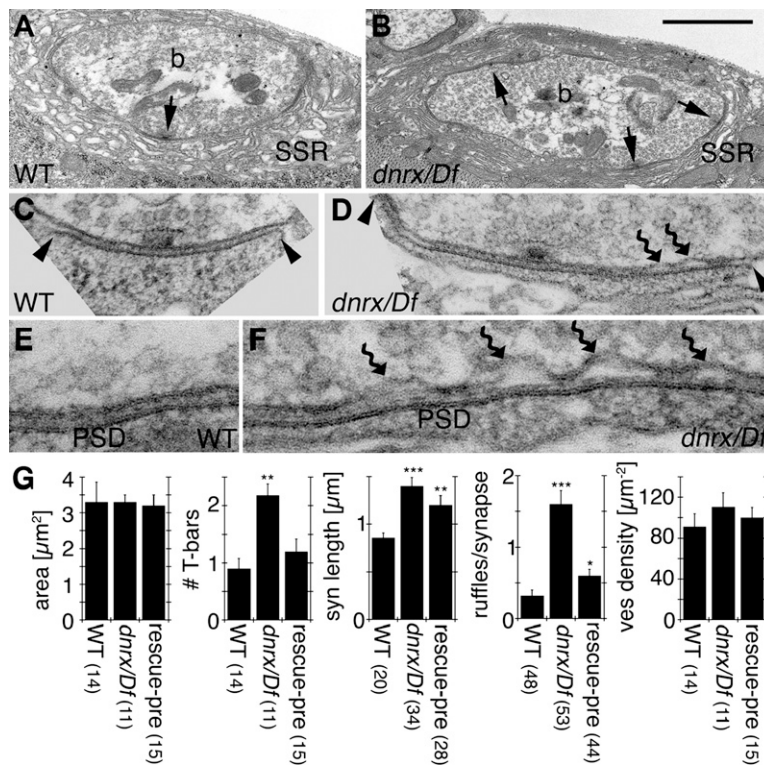


Figure 7. Ultrastructural Analysis of Type I Synaptic Bouton in *dnrx* Mutants

(A–F) TEM micrographs of (A, C, and E) wild-type and (B, D, and F) *dnrx²⁷³/Df* mutants.

(A) and (B) are low-magnification views of synaptic bouton midlines (b), showing the presynaptic active zones (arrows) and post-synaptic SSR. Note that in *dnrx²⁷³/Df* mutants the number of active zones is increased.

(C and D) Higher-magnification view of the PSD (between arrowheads) and its juxtaposed PRD containing a T bar. In *dnrx²⁷³/Df* mutants, both PSDs and PRDs are much longer than wild-type. In addition, the presynaptic membrane shows signs of detachment from the PSD (curved arrows).

(E and F) High-magnification view of a region of the PRD and apposed PSD. While in wild-type the synaptic cleft between the PSD and PRD has a constant size, in *dnrx²⁷³/Df* mutants this size is variable, due to the presence of detachments of the presynaptic membrane (curved arrows). Also note that at sites of detachments the PRD no longer displays its typical electron density.

(G) Morphometric analysis of synaptic boutons, showing bouton midline area, number of T bars, synapse length, number of ruffles/synapse, and vesicle density. Numbers in parenthesis below genotypes correspond to the number of samples (see Experimental Procedures). *** $p < 0.001$, ** $p < 0.01$, and * $p < 0.05$. Data are mean \pm SEM.

Scale bars, 1 μm (A and B), 0.2 μm (C and D), 0.1 μm (E and F).

release could be altered in *dnrx* mutants. For these experiments, the amplitude of evoked responses was measured at three Ca^{2+} concentrations: 0.5, 0.75, and 1 mM. As previously described, there was a significant decrease in EJP amplitude in *dnrx* mutants at 0.5 mM Ca^{2+} . Surprisingly, however, this defect was completely restored when recordings were performed at 1 mM Ca^{2+} (Figure 8D).

The change in the slope of Ca^{2+} dependency of release could be due to either changes in Ca^{2+} coupling to exocytosis or an abnormality in the distribution of presynaptic Ca^{2+} channels. To address this issue, we examined the distribution of cacophony (Cac), the presynaptic N-type Ca^{2+} channel at these synapses (Smith et al., 1996; Littleton and Ganetzky, 2000). Ca^{2+} channels are extremely sensitive to fixation. Therefore, we used a GFP-tagged Cac transgene (*Cac-GFP*) to visualize Ca^{2+} channels in vivo. Previous studies have demonstrated that expression of this transgene faithfully replicates endogenous Cac distribution and function (Kawasaki et al., 2004). *Cac-GFP* transgene was expressed in neurons using *elav-Gal4*, and samples were imaged live in a spinning disk confocal microscope. There were no statistically significant differences either in the size or intensity of Cac-GFP clusters between controls and *dnrx* mutants (Figure S3), indicating that the defect in Ca^{2+} sensitivity is most likely the result of changes in coupling rather than Ca^{2+} channel distribution.

DISCUSSION

Although cell adhesion molecules have long been postulated and in several cases have been shown to be major participants in synapse development and plasticity, the impact of their function and the molecular mechanisms that they activate remain a puzzle. Particularly intriguing is the function of neuroligins, which may provide clues to our understanding of synapse organization. We have isolated null mutants in the single *Drosophila dnrx* gene. We show that *dnrx* mutants have striking abnormalities in synapse development and function. A recent study reported that *Drosophila* neuroligin is required for synapse formation in the adult CNS (Zeng et al., 2007). In the current study, we not only demonstrate a primary role of DNRX in regulating the formation of synapses, but also reveal the crucial role of DNRX in the proper development of active zones and regulating synaptic function in an intact organism, thus providing insights into understanding the function of neuroligins in vivo.

Function of DNRX during Synapse Development

Our studies provide compelling evidence that DNRX plays a prime role during the expansion of the NMJ and, in particular, in defining the cytoarchitecture of the active zones within synaptic boutons. First, in *dnrx*

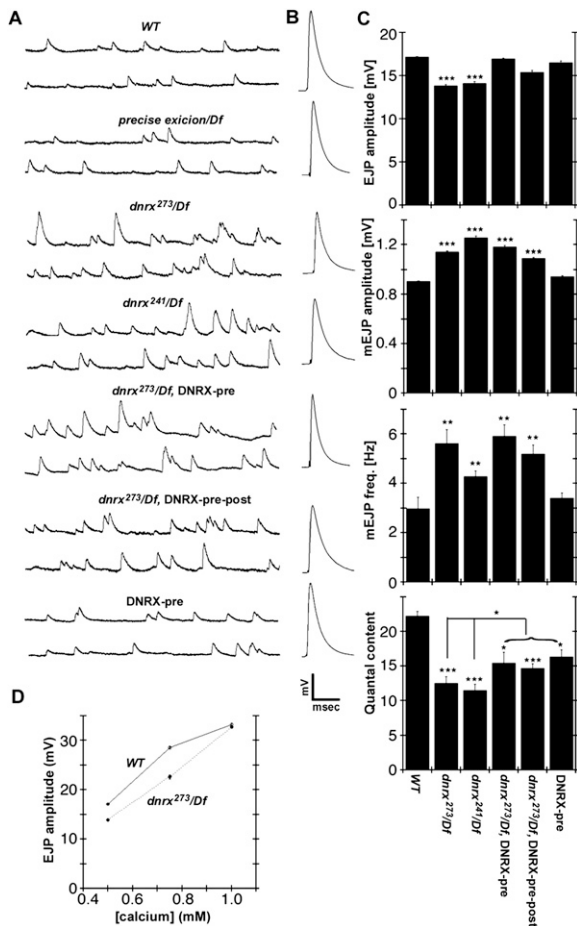


Figure 8. Electrophysiological Analysis of NMJs
 (A) Representative traces of mEJPs in the genotypes indicated. Note that both the frequency and amplitude of mEJPs are enhanced in *dnrx*/Df mutants.
 (B) Representative traces of evoked responses, showing a decrease in peak amplitude in *dnrx*/Df mutants. Calibration scale: 3 mV and 230 ms (A); 6 mV and 10 ms (B).
 (C) Quantification of EJP and mEJP amplitude, mEJP frequency, and quantal content (EJP/mEJP amplitude). ****p* < 0.001; ***p* < 0.01; and **p* < 0.05. Data are mean ± SEM.
 (D) EJP amplitude as a function of external Ca²⁺ concentration in wild-type and *dnrx* mutants.

mutants, synaptic bouton proliferation is severely disrupted, and therefore NMJ expansion is significantly stunted. Second, DNRX gain of function promotes the formation of new boutons in a gene-dosage-dependent manner. Third, the ultrastructural analyses show that PRDs are not apposed normally to PSDs displaying signs of abnormal adhesion to the PSD, although every PRD is exactly juxtaposed to the PSD. Fourth, in *dnrx* mutants, critical components of the presynaptic compartment, such as synaptic vesicle proteins and active zone components, are ectopically localized within axons. Fifth, the distribution of GluRs at the PSD is abnormally large, although this phenotype may arise as a consequence of

the presynaptic defects observed in *dnrx* mutants (discussed below).

The great majority of abnormal phenotypes in *dnrx* mutants could be completely rescued by expressing a wild-type *dnrx* transgene in neurons; although in some instances the rescue was partial. However, even in the later case, expressing *dnrx* in both muscles and neurons did not further improve the residual abnormalities, suggesting that *dnrx* functions primarily if not exclusively in the presynaptic compartment.

The partial rescue of some of the phenotypes, such as the defects in mEJPs and the morphology of active zones, might be due to the high sensitivity of these processes to the right levels and correct temporal expression of *dnrx*, which is not completely mimicked by the UAS/Gal4 system. This view is supported by the observation that overexpression of *dnrx* in a wild-type background also decreased quantal content, suggesting that increased *dnrx* dosage may have detrimental effects on synapse structure and/or function. However, the data strongly support that the abnormal phenotypes arise from the lack of *dnrx*. First, all our experiments were carried out in mutants over a deficiency chromosome in an independent genetic background. Second, a precise excision of the *P* element did not show any of the mutant phenotypes. Together these data establish a specific role for DNRX in proper synaptic development.

Role of DNRX in Active Zone Morphogenesis

One of our important findings is that *dnrx* mutants displayed defective active zones with larger PRD, and especially containing regions of detachment from the PSD. These detachment sites implicate DNRX as a mediator of cell adhesion between the pre- and the postsynaptic cell, in accordance with previous suggestions in mammalian neurons (Scheiffele et al., 2000; Graf et al., 2004; Dean et al., 2003). While a complete detachment of active zones is not observed, *dnrx* mutants have a significant decrease in the number of boutons. This raises the possibility that the phenotypes we observe are from those boutons that are maintained and that a more drastic consequence is a failure to form synaptic boutons. Nevertheless, the lack of complete detachment of active zones in *dnrx* null mutants suggests that DNRX, although an important synapse-organization molecule, is not sufficient for *trans*-synaptic cell adhesion.

Another notable phenotype in *dnrx* mutants was the presence of enlarged PRDs and increased number of T bars. A major feature of *Drosophila* larval NMJ is its ability to compensate for decreased postsynaptic responses by upregulating neurotransmitter release. For instance, a decrease in the number of postsynaptic GluRs results in an increase in neurotransmitter release, thus maintaining the amplitude of evoked responses (Petersen et al., 1997). It is plausible that the enlarged PRDs and increase in number of T bars in *dnrx* mutants are a compensatory mechanism to adjust for defective presynaptic cell adhesion and/or reduced neurotransmitter release (Murthy

et al., 2001; Stewart et al., 1996). In support of this notion, in *dnrx* mutants there was a 50% decrease in synaptic bouton number, but this was accompanied by a 2-fold increase in the number of T bars, such that the total number of T bars/NMJ remained constant, despite the changes in bouton number. Similarly, defective presynaptic cell adhesion and/or reduced neurotransmitter release could lead to an increase in GluR accumulation (O'Brien et al., 1998). In our studies, we found that the length of the PSD was enlarged in *dnrx* mutants as well as the distribution of GluR clusters.

Functional Consequences of Altering DNRX Function

The above structural abnormalities were accompanied by corresponding functional deficits. In *dnrx* mutants, the frequency of mEJPs was strikingly increased. Further, although the T bars were rescued by expression of a *dnrx* transgene, the length of the PRDs was not, and a similar lack of rescue was observed for mEJP frequency. Thus, there appears to be a notable correlation between the size of the PRD and mEJP frequency, perhaps due to increased probability of synaptic vesicle release with increased synapse size. In addition, we also observed a substantial increase in mEJP amplitude. Two factors may contribute to this change. First, the distribution of GluR clusters was enlarged, while the GluR intensity remained unchanged, suggesting that more GluRs were accumulated at mutant synapses. An additional contributing factor is that mEJP frequency was increased, and we observed instances of summation.

Overall, despite the increase in PRD size and the maintenance of overall T bar number, evoked events had a decrease in amplitude and quantal content. Recent studies have suggested that a major constituent of the T bars is BRP/CAST (Kittel et al., 2006; Wagh et al., 2006). In *brp* mutants, T bars fail to form, but PRDs appear unaltered. Further, although EJP amplitude is decreased, mEJP amplitude and frequency are normal. This has led to the model that T bars per se are not required for synaptic transmission but that they regulate the efficiency of transmission. In *dnrx* mutants, PRDs are disproportionately large, which could result in asynchronous release, leading to an EJP with decreased amplitude. It is also possible that the presynaptic membrane detachments observed in *dnrx* mutants could contribute to the functional impairment of neurotransmitter release.

A recent study demonstrated that in *dnrx* mutant larvae associative learning is impaired in an olfactory choice paradigm (Zeng et al., 2007). However, in this study, larval locomotion was not assessed. Our study showing that locomotor behavior is impaired in *dnrx* mutants raises the possibility that the poor performance of mutant larvae in the conditioning assay might also result from the locomotor abnormalities. Zeng et al. also reported that the number of T bars in the calyx of the mushroom bodies, the learning centers of the fly, was reduced in adult flies. In contrast, we found a significant increase in the number

of T bar/bouton, and since *dnrx* mutants have fewer boutons, this translated in the maintenance of T bar number per NMJ. The differing results might be due to different mechanisms regulating T bar formation in the two tissues.

DNRX Function in Relation to Mammals

The presence of a neurexin in *Drosophila* strengthened the view that neurexins are highly conserved across species (Tabuchi and Sudhof, 2002). The synaptic DNRX expression pattern and its function show remarkable parallels with mammalian neurexins. Moreover, the proteins that have been shown to interact with mammalian neurexins also have homologs in *Drosophila*, which further supports the idea that the function of neurexins and underlying signaling mechanism are evolutionarily conserved. Among these, *Drosophila* neuroligin and/or dystroglycan (Dg) (Deng et al., 2003) might be potential DNRX ligands. *Drosophila* neuroligin transcription exhibits almost an identical temporal and spatial expression pattern as *dnrx* during embryonic stages (unpublished data). *dg* is highly expressed in the somatic musculature of embryos (BDGP gene expression report). *dg* mutants are embryonic lethal, and perturbation of Dg function by RNAi as well as genetic interaction studies suggest an involvement of Dg in muscle maintenance and axonal pathfinding in adult flies (Shcherbata et al., 2007). Future studies on the identification and characterization of DNRX binding partners in *Drosophila* should provide additional insights into the mechanisms by which neurexins function in synapse development and function.

Extensive cell culture studies of neurexins and neuroligins and functional studies using α -neurexin knockout mice have established a central role for neurexins as synaptic adhesive and organizing molecules. Our studies on DNRX provide evidence in an intact organism that neurexin is required for important aspects of synapse development and function. Our DNRX gain-of-function analysis reveals that overexpression of DNRX is sufficient to promote the formation of synaptic boutons in vivo, in agreement with the findings from cell culture studies suggesting that neurexin-neuroligin *trans*-synaptic complexes can induce pre- and postsynaptic differentiation and synapse formation (Graf et al., 2004; Scheiffele et al., 2000; Dean et al., 2003; Chih et al., 2005). Moreover, the accumulations of synaptic vesicle and active zone proteins along axons of *dnrx* null mutants further support the notion that neurexins may recruit or organize synaptic proteins or organelles during presynaptic differentiation. Phenotypic analyses of α -neurexin knockout mice demonstrated that α -neurexin is essential for synaptic transmission in a process that depends on presynaptic voltage-dependent Ca^{2+} channels (Missler et al., 2003; Zhang et al., 2005). However, triple-knockout mice have normal surface expression of Ca^{2+} channels. These findings have led to the hypothesis that neurexins regulate the coupling between Ca^{2+} channels and the neurotransmitter release machinery. Similarly, in *dnrx* null mutants we found that the Ca^{2+} sensitivity of evoked responses was abnormal,

but the distribution or levels of presynaptic Ca^{2+} channel Cac was unchanged, consistent with the above hypothesis. Notably, Syt I, a synaptic vesicle protein that binds Ca^{2+} and has been proposed to function as a Ca^{2+} sensor (Geppert et al., 1994; Yoshihara and Littleton, 2002) during synaptic vesicle exocytosis, was partly mislocalized to axons in *dnrx* mutants. Furthermore, the structure of active zones was impaired in these mutants. Therefore, the organization of active zone proteins including the assembly of neurotransmitter release machinery might be affected in *dnrx* mutants.

In conclusion, our studies in *Drosophila* demonstrate that DNRX is required for both synapse development and function and, in particular, for proper formation of active zones. Our studies provide compelling evidence for an in vivo role of neurexins in the modulation of synaptic architecture and adhesive interactions between pre- and postsynaptic compartments.

EXPERIMENTAL PROCEDURES

Cloning of *dnrx* Full-Length cDNA

A radio-labeled *dnrx* EST (LP03809) was used to screen a *Drosophila* 0–20 hr embryo cDNA library. Overlapping partial cDNA clones were isolated, sequenced, and compiled as a cDNA sequence of 5738 base pairs (GenBank accession number EF460788), which comprises an open reading frame of 5520 base pairs with 5' and 3' UTR.

In Situ Hybridization

A HindIII-Sall fragment of *dnrx* cDNA clone encoding the second LamG-EGF-LamG-domain repeat, and a PstI-NotI fragment encoding the last-LamG-domain-cytoplasmic-region were cloned into pBlue-script vector. The two resulting clones were linearized. Antisense and sense RNA probes were synthesized by using T7 and T3 RNA polymerases, labeled with digoxigenin-UTP (Roche), and used for in situ hybridization following standard protocols.

Production of DNRX Antibody

A guinea pig polyclonal antibody against DNRX was generated against a recombinant protein containing the cytoplasmic region of DNRX fused with a His₆ tag at the N terminus. The sera were affinity purified using a recombinant protein containing the same cytoplasmic tail fused to glutathione S-transferase. The purified anti-DNRX antibody was used at a dilution of 1:500 for tissue staining and 1:1000 for western blot analysis.

Generation of *dnrx* Mutants

XP d08766 (Thibault et al., 2004), a *P* element inserted ~200 bp upstream of *dnrx*, was used to carry out an excision screen. To increase the frequency of large deletions, the excision screen was carried out in *mus309* background (Adams et al., 2003; McVey et al., 2004). Briefly, *XP d08766* was first recombined to *mus309^{NI}*. *mus309^{NI} XPd08766/TM6* *Tb* males were massively mated with *mus309^{D3} Sb Δ2-3/TM6* *Tb* females. The *mus309^{NI} XPd08766/mus309^{D3} Sb Δ2-3* males were individually crossed with *D/TM6* *Tb* females. *w* male progeny was selected and individually crossed with *Df(3R)5C1/TM3 Sb Kr::GFP*. Single *ΔXP/Df(3R)5C1* male flies were subject to PCR to select imprecise excisions, and *ΔXP/TM3 Sb Kr::GFP* were used to establish stock lines. *dnrx* deletions were obtained by selecting imprecise excisions downstream of the *P* element insertion site using primer pairs covering the whole *dnrx* locus. The following primer pairs were used to confirm *dnrx²⁷³* and *dnrx²⁴¹* alleles with a common 5' primer (5'-ACGCGTCGCGCTAAAATC CAGCCCG-3'); and separate 3' primers (*dnrx²⁷³*, 5'-CGTATGAG

TGCTTGGAGCGGAA-3'; and *dnrx²⁴¹*, 5'-AGCCGGTGCCGATGTCTA TGACGAA-3').

Fly Stocks and Genetics

dnrx mutant alleles *dnrx²⁷³*, *dnrx²⁴¹*, and *Df(3R)5C1* (a deficiency that removes *dnrx*) were balanced over *TM3 Sb Kr::GFP*. *dnrx* mutants were identified by selecting third-instar larvae without GFP expression. *UAS-dnrx* transgenic flies were generated by cloning the entire *dnrx* full-length cDNA into *pUASP* vector for germ line transformation. Gal4 lines used for DNRX overexpression and rescue experiments were *C380*, which drives Gal4 expression mainly in motoneurons (Budnik et al., 1996), and *elav*, which drives Gal4 expression in all neurons (Lin and Goodman, 1994).

Larval Locomotor Assay

The larval locomotor assay was performed as described by Connolly and Tully (1998). Individual larvae were placed in the center of a 145 mm diameter Petri dish, with 3% agar covering the bottom and a 0.5 × 0.5 cm square grid marked on the lid. The number of grid line crossings within a 30 s time window was recorded six times.

Immunohistochemistry, Confocal Microscopy, and Morphological Quantification

Preparation and antibody staining for whole-mount embryos and dissected wandering third-instar larvae were performed as described by Bellen and Budnik (2000). Dissected larval NMJs were fixed in Bouin's fixative for 15 min. The following antibodies were used: guinea pig anti-DNRX (1:500), rabbit anti-DPAK (1:2000, N. Harden, Simon Fraser University, Canada; Harden et al., 1996), rabbit anti-NWK (1:2000, B. Ganetzky, University of Wisconsin, Madison; Coyle et al., 2004), rabbit anti-Syt I (1:500, H. Bellen, Baylor College of Medicine, Houston; Littleton et al., 1993); rabbit anti-GluRIII (1:2000, A. DiAntonio, Washington University, St. Louis; Marrus et al., 2004); guinea pig anti-Dap160 (1:2000, H. Bellen, Baylor College of Medicine, Houston; Koh et al., 2004), monoclonal anti-DLG (1:500), anti-BRP (1:500), anti-GluRIIA (1:50), and anti-FASII (1:100) from Developmental Studies Hybridoma Bank, University of Iowa. Secondary antibodies conjugated to Alexa 488, 568, and 647 (Invitrogen-Molecular Probes) were used at 1:400. Fluorescence-conjugated anti-HRP (Jackson Immuno Labs) antibodies were used at 1:50.

DNRX signal at the NMJ was detected by using the VECTASTAIN ABC system (Vector Laboratories) and Tyramide Signal Amplification (TSA, Invitrogen-Molecular Probes). Double staining of NMJ with anti-DNRX and a second primary antibody was performed as follows. Briefly, fixed larvae were washed in PBT (PBS containing 0.3% triton X-100) and blocked for 1 hr with 1% blocking reagent (TSA kit, Invitrogen-Molecular Probes). Blocked samples were incubated with anti-DNRX and a second primary antibody overnight at 4°C. After washes with PBT, the samples were incubated with biotinylated goat anti-guinea pig antibody (1:400, Vector Laboratories) and a fluorescent secondary antibody. The incubation was followed by washes with PBT and 1 hr incubation in ABC reagent (1:250 in 2% BSA/PBT, diluted 30 min before use, Vector laboratories). Six subsequent washes with PBT and one with PBS were followed by tyramide labeling according to the manufacturer's instructions.

Confocal images were acquired using a Bio-Rad Radiance 2000 confocal microscope with LaserSharp2000 software. Samples for each experiment were processed simultaneously and imaged using the same settings. For Cac-GFP live imaging, larvae were mounted on the slides and the images were acquired from live body wall muscle preparations with an Impropvision spinning disc confocal microscope.

Quantification of bouton number was performed at muscles 6/7 and muscle 4 of abdominal segment 3. Total boutons at NMJ6/7 and type Ib boutons at NMJ4 were visualized by staining of body wall muscle preparations with anti-HRP. For quantification of axonal Syt accumulation, the length of SNb axon innervating muscles 12/13 or ISN axon and its primary branches innervating muscle 4 in abdominal segment

3 or 4 was measured; the number of Syt puncta along these axons was counted and further divided by the axon length. Statistical analyses were performed using InStat 3.00 (Graphpad).

Electron Microscopy

Body wall muscles were prepared for TEM as previously described (Torroja et al., 1999). Synaptic boutons were serially sectioned and photographed at 10,000–50,000 \times using a Philips CM10 TEM. For morphometric analysis, the cross-section corresponding to the bouton midline (cross-section of largest diameter) was identified, the negative scanned at 60,000 \times , and used for quantification using Image J as in Budnik et al. (1996). The number of samples used were three wild-type controls (14 boutons), three *dnrx/Df* (11 boutons), and three rescue animals (15 boutons). For analysis of synapse length and synapse ruffles, sections other than the midline section were also considered for quantification, as long as pre- and postsynaptic densities as well as the synaptic cleft were clearly visualized, had consistent thickness, and lacked the blurry appearance of membranes cut at a tangential plane. Statistical analysis was performed using a two-tailed Student's *t* test.

Electrophysiology

Electrophysiology recordings were performed as in Ashley et al. (2005). Briefly, third-instar larvae were dissected under cold 0.3 mM calcium HL-3 saline and then perfused continuously with 0.5 mM calcium HL-3 saline at 22°C. Muscle 6 in segment A3 was then impaled with a 15–20 M Ω glass electrodes. Only samples with resting membrane potentials between –60 mV and –63 mV were used for analysis. Data were collected using an Axoclamp2A (Molecular Devices), filtered at 1 kHz, and digitized with an Instrutech (Port Washington) ITC-16 computer interface using Pulse software (HEKA Elektronik, Lambrrecht/Pfalz). Spontaneous and evoked events were then measured using Mini Analysis software (Synaptosoft). Statistical analysis was performed using the Student's *t* test.

Quantification of GluR IIA Intensity

NMJ staining of *dnrx* mutant and wild-type larvae with monoclonal anti-GluRIIA and FITC anti-HRP was performed in the same tube. Several regions of NMJ4 from three animals for each genotype were scanned by confocal microscope. Confocal stacks were acquired using the same settings that prevented pixel saturation with 0.25 μ m steps through entire synaptic boutons. Images were processed using Velocity 4.1 (Improvision). Total volumes of synaptic boutons outlined by HRP staining and the fluorescence of GluRIIA staining were calculated. Total GluRIIA fluorescence divided by total volumes of boutons represented GluR intensity.

Supplemental Data

The Supplemental Data for this article can be found online at <http://www.neuron.org/cgi/content/full/55/5/741/DC1/>.

ACKNOWLEDGMENTS

We thank Drs. Hugo Bellen, Steve Crews, and Alan Fanning for comments and discussions. We also thank Dr. Michael Chua for assistance on quantification analysis of GluR; Norberto Gherbesi for assistance in ultrastructural analysis; Raehum Paik and Anilkumar Pillai for technical assistance; and the staff of the UM Massed Electron Microscopy Facility. Finally, we thank Drs. Hugo Bellen, Jeff Sekelsky, Aaron DiAntonio, Nicholas Harden, Barry Ganetzky, Wu-Min Deng, and the Bloomington Stock Center (supported by Grant No. 0342468) for many valuable reagents. This work was supported by grants from the National Institute of General Medical Sciences (GM63074, to M.A.B.), National Institute of Neurological Disorders and Stroke (NS050356, to M.A.B.), National Institute of Mental Health (MH070000, to V.B.), and funds from the State of North Carolina (to M.A.B.).

Received: March 9, 2007

Revised: July 17, 2007

Accepted: August 7, 2007

Published: September 5, 2007

REFERENCES

- Adams, M.D., Celniker, S.E., Holt, R.A., Evans, C.A., Gocayne, J.D., Amanatides, P.G., Scherer, S.E., Li, P.W., Hoskins, R.A., Galle, R.F., et al. (2000). The genome sequence of *Drosophila melanogaster*. *Science* 287, 2185–2195.
- Adams, M.D., McVey, M., and Sekelsky, J.J. (2003). *Drosophila* BLM in double-strand break repair by synthesis-dependent strand annealing. *Science* 299, 265–267.
- Ashley, J., Packard, M., Ataman, B., and Budnik, V. (2005). Fasciclin II signals new synapse formation through amyloid precursor protein and the scaffolding protein dX11/Mint. *J. Neurosci.* 25, 5943–5955.
- Atasoy, D., Schoch, S., Ho, A., Nadasy, K.A., Liu, X., Zhang, W., Mukherjee, K., Nosyreva, E.D., Fernandez-Chacon, R., Missler, M., et al. (2007). Deletion of *CASK* in mice is lethal and impairs synaptic function. *Proc. Natl. Acad. Sci. USA* 104, 2525–2530.
- Banerjee, S., Pillai, A.M., Paik, R., Li, J., and Bhat, M.A. (2006). Axonal ensheathment and septate junction formation in the peripheral nervous system of *Drosophila*. *J. Neurosci.* 26, 3319–3329.
- Baumgartner, S., Littleton, J.T., Broadie, K., Bhat, M.A., Harbecke, R., Lengyel, J.A., Chiquet-Ehrismann, R., Prokop, A., and Bellen, H.J. (1996). A *Drosophila* neurexin is required for septate junction and blood-nerve barrier formation and function. *Cell* 87, 1059–1068.
- Bellen, H.J., and Budnik, V. (2000). The neuromuscular junction. In *Drosophila*, A Laboratory Manual, M. Ashburner, S. Hawley, and B. Sullivan, eds. (Cold Spring Harbor, NY: Cold Spring Harbor Laboratory), pp. 175–199.
- Bellen, H.J., Lu, Y., Beckstead, R., and Bhat, M.A. (1998). Neurexin IV, caspr and paranodin—novel members of the neurexin family: encounters of axons and glia. *Trends Neurosci.* 21, 444–449.
- Bhat, M.A., Rios, J.C., Lu, Y., Garcia-Fresco, G.P., Ching, W., St Martin, M., Li, J., Einheber, S., Chesler, M., Rosenbluth, J., et al. (2001). Axon-glia interactions and the domain organization of myelinated axons requires neurexin IV/Caspr/Paranodin. *Neuron* 30, 369–383.
- Biederer, T., and Sudhof, T.C. (2000). Mints as adaptors. Direct binding to neurexins and recruitment of munc18. *J. Biol. Chem.* 275, 39803–39806.
- Boucard, A.A., Chubykin, A.A., Comoletti, D., Taylor, P., and Sudhof, T.C. (2005). A splice code for trans-synaptic cell adhesion mediated by binding of neuroligin 1 to alpha- and beta-neurexins. *Neuron* 48, 229–236.
- Budnik, V., Koh, Y.H., Guan, B., Hartmann, B., Hough, C., Woods, D., and Gorczyca, M. (1996). Regulation of synapse structure and function by the *Drosophila* tumor suppressor gene *dlg*. *Neuron* 17, 627–640.
- Chih, B., Engelman, H., and Scheiffele, P. (2005). Control of excitatory and inhibitory synapse formation by neuroligins. *Science* 307, 1324–1328.
- Chih, B., Gollan, L., and Scheiffele, P. (2006). Alternative splicing controls selective trans-synaptic interactions of the neuroligin-neurexin complex. *Neuron* 51, 171–178.
- Comoletti, D., Flynn, R.E., Boucard, A.A., Demeler, B., Schirf, V., Shi, J., Jennings, L.L., Newlin, H.R., Sudhof, T.C., and Taylor, P. (2006). Gene selection, alternative splicing, and post-translational processing regulate neuroligin selectivity for beta-neurexins. *Biochemistry* 45, 12816–12827.
- Connolly, J.B., and Tully, T. (1998). Behaviour, learning, and memory. In *Drosophila*, A Practical Approach, D.B. Roberts, ed. (New York: Oxford University Press), pp. 265–317.

- Coyle, I.P., Koh, Y.H., Lee, W.C., Slind, J., Fergestad, T., Littleton, J.T., and Ganetzky, B. (2004). Nervous wreck, an SH3 adaptor protein that interacts with Wsp, regulates synaptic growth in *Drosophila*. *Neuron* 41, 521–534.
- Dean, C., Scholl, F.G., Choih, J., DeMaria, S., Berger, J., Isacoff, E., and Scheiffele, P. (2003). Neurexin mediates the assembly of presynaptic terminals. *Nat. Neurosci.* 6, 708–716.
- Deng, W.M., Schneider, M., Frock, R., Castillejo-Lopez, C., Gaman, E.A., Baumgartner, S., and Ruohola-Baker, H. (2003). Dystroglycan is required for polarizing the epithelial cells and the oocyte in *Drosophila*. *Development* 130, 173–184.
- Favre-Sarrailh, C., Banerjee, S., Li, J., Hortsch, M., Laval, M., and Bhat, M.A. (2004). *Drosophila* contactin, a homolog of vertebrate contactin, is required for septate junction organization and paracellular barrier function. *Development* 131, 4931–4942.
- Fu, Z., Washbourne, P., Ortinski, P., and Vicini, S. (2003). Functional excitatory synapses in HEK293 cells expressing neuroligin and glutamate receptors. *J. Neurophysiol.* 90, 3950–3957.
- Geppert, M., Goda, Y., Hammer, R.E., Li, C., Rosahl, T.W., Stevens, C.F., and Sudhof, T.C. (1994). Synaptotagmin I: a major Ca²⁺ sensor for transmitter release at a central synapse. *Cell* 79, 717–727.
- Gerrow, K., and El-Husseini, A. (2006). Cell adhesion molecules at the synapse. *Front. Biosci.* 11, 2400–2419.
- Graf, E.R., Zhang, X., Jin, S.X., Linhoff, M.W., and Craig, A.M. (2004). Neurexins induce differentiation of GABA and glutamate postsynaptic specializations via neuroligins. *Cell* 119, 1013–1026.
- Graf, E.R., Kang, Y., Hauner, A.M., and Craig, A.M. (2006). Structure function and splice site analysis of the synaptogenic activity of the neurexin-1 beta LNS domain. *J. Neurosci.* 26, 4256–4265.
- Griffith, L.C., and Budnik, V. (2006). Plasticity and second messengers during synapse development. *Int. Rev. Neurobiol.* 75, 237–265.
- Harden, N., Lee, J., Loh, H.Y., Ong, Y.M., Tan, I., Leung, T., Manser, E., and Lim, L. (1996). A *Drosophila* homolog of the Rac- and Cdc42-activated serine/threonine kinase PAK is a potential focal adhesion and focal complex protein that colocalizes with dynamic actin structures. *Mol. Cell. Biol.* 16, 1896–1908.
- Hata, Y., Davletov, B., Petrenko, A.G., Jahn, R., and Sudhof, T.C. (1993). Interaction of synaptotagmin with the cytoplasmic domains of neuexins. *Neuron* 10, 307–315.
- Hata, Y., Butz, S., and Sudhof, T.C. (1996). CASK: a novel dlg/PSD95 homolog with an N-terminal calmodulin-dependent protein kinase domain identified by interaction with neuexins. *J. Neurosci.* 16, 2488–2494.
- Ho, A., Morishita, W., Hammer, R.E., Malenka, R.C., and Sudhof, T.C. (2003). A role for Mints in transmitter release: Mint 1 knockout mice exhibit impaired GABAergic synaptic transmission. *Proc. Natl. Acad. Sci. USA* 100, 1409–1414.
- Hummel, T., Krukkert, K., Roos, J., Davis, G., and Klambt, C. (2000). *Drosophila* Futsch/22C10 is a MAP1B-like protein required for dendritic and axonal development. *Neuron* 26, 357–370.
- Ichtchenko, K., Hata, Y., Nguyen, T., Ullrich, B., Missler, M., Moomaw, C., and Sudhof, T.C. (1995). Neuroligin 1: a splice site-specific ligand for beta-neuexins. *Cell* 81, 435–443.
- Irie, M., Hata, Y., Takeuchi, M., Ichtchenko, K., Toyoda, A., Hirao, K., Takai, Y., Rosahl, T.W., and Sudhof, T.C. (1997). Binding of neuroligins to PSD-95. *Science* 277, 1511–1515.
- Kattenstroth, G., Tantalaki, E., Sudhof, T.C., Gottmann, K., and Missler, M. (2004). Postsynaptic N-methyl-D-aspartate receptor function requires alpha-neuexins. *Proc. Natl. Acad. Sci. USA* 101, 2607–2612.
- Kawasaki, F., Zou, B., Xu, X., and Ordway, R.W. (2004). Active zone localization of presynaptic calcium channels encoded by the cacophony locus of *Drosophila*. *J. Neurosci.* 24, 282–285.
- Kittel, R.J., Wichmann, C., Rasse, T.M., Fouquet, W., Schmidt, M., Schmid, A., Wagh, D.A., Pawlu, C., Kellner, R.R., Willig, K.I., et al. (2006). Bruchpilot promotes active zone assembly, Ca²⁺ channel clustering, and vesicle release. *Science* 312, 1051–1054.
- Koh, T.W., Verstreken, P., and Bellen, H.J. (2004). Dap160/intersectin acts as a stabilizing scaffold required for synaptic development and vesicle endocytosis. *Neuron* 43, 193–205.
- Kumar, S., Tamura, K., and Nei, M. (2004). MEGA3: Integrated software for Molecular Evolutionary Genetics Analysis and sequence alignment. *Brief. Bioinform.* 5, 150–163.
- Lahey, T., Gorczyca, M., Jia, X.X., and Budnik, V. (1994). The *Drosophila* tumor suppressor gene *dlg* is required for normal synaptic bouton structure. *Neuron* 13, 823–835.
- Levinson, J.N., Chery, N., Huang, K., Wong, T.P., Gerrow, K., Kang, R., Prange, O., Wang, Y.T., and El-Husseini, A. (2005). Neuroligins mediate excitatory and inhibitory synapse formation: involvement of PSD-95 and neurexin-1beta in neuroligin-induced synaptic specificity. *J. Biol. Chem.* 280, 17312–17319.
- Lin, D.M., and Goodman, C.S. (1994). Ectopic and increased expression of Fasciclin II alters motoneuron growth cone guidance. *Neuron* 13, 507–523.
- Littleton, J.T., and Ganetzky, B. (2000). Ion channels and synaptic organization: analysis of the *Drosophila* genome. *Neuron* 26, 35–43.
- Littleton, J.T., Bellen, H.J., and Perin, M.S. (1993). Expression of synaptotagmin in *Drosophila* reveals transport and localization of synaptic vesicles to the synapse. *Development* 118, 1077–1088.
- Marie, B., Sweeney, S.T., Poskanzer, K.E., Roos, J., Kelly, R.B., and Davis, G.W. (2004). Dap160/intersectin scaffolds the periaxonal zone to achieve high-fidelity endocytosis and normal synaptic growth. *Neuron* 43, 207–219.
- Marrus, S.B., Portman, S.L., Allen, M.J., Moffat, K.G., and DiAntonio, A. (2004). Differential localization of glutamate receptor subunits at the *Drosophila* neuromuscular junction. *J. Neurosci.* 24, 1406–1415.
- McVey, M., Larocque, J.R., Adams, M.D., and Sekelsky, J.J. (2004). Formation of deletions during double-strand break repair in *Drosophila* DmBlm mutants occurs after strand invasion. *Proc. Natl. Acad. Sci. USA* 101, 15694–15699.
- Meyer, G., Varoqueaux, F., Neeb, A., Oschlies, M., and Brose, N. (2004). The complexity of PDZ domain-mediated interactions at glutamatergic synapses: a case study on neuroligin. *Neuropharmacology* 47, 724–733.
- Missler, M., and Sudhof, T.C. (1998). Neuexins: three genes and 1001 products. *Trends Genet.* 14, 20–26.
- Missler, M., Zhang, W., Rohlmann, A., Kattenstroth, G., Hammer, R.E., Gottmann, K., and Sudhof, T.C. (2003). Alpha-neuexins couple Ca²⁺ channels to synaptic vesicle exocytosis. *Nature* 423, 939–948.
- Murthy, V.N., Schikorski, T., Stevens, C.F., and Zhu, Y. (2001). Inactivity produces increases in neurotransmitter release and synapse size. *Neuron* 32, 673–682.
- Nam, C.I., and Chen, L. (2005). Postsynaptic assembly induced by neuexin-neuroligin interaction and neurotransmitter. *Proc. Natl. Acad. Sci. USA* 102, 6137–6142.
- O'Brien, R.J., Kamboj, S., Ehlers, M.D., Rosen, K.R., Fischbach, G.D., and Haganir, R.L. (1998). Activity-dependent modulation of synaptic AMPA receptor accumulation. *Neuron* 21, 1067–1078.
- Peles, E., Joho, K., Plowman, G.D., and Schlessinger, J. (1997). Close similarity between *Drosophila* neuexin IV and mammalian Caspr protein suggests a conserved mechanism for cellular interactions. *Cell* 88, 745–746.
- Petersen, S.A., Fetter, R.D., Noordermeer, J.N., Goodman, C.S., and DiAntonio, A. (1997). Genetic analysis of glutamate receptors in *Drosophila* reveals a retrograde signal regulating presynaptic transmitter release. *Neuron* 19, 1237–1248.

- Poliak, S., Gollan, L., Martinez, R., Custer, A., Einheber, S., Salzer, J.L., Trimmer, J.S., Shrager, P., and Peles, E. (1999). Caspr2, a new member of the neurexin superfamily, is localized at the juxtaparanodes of myelinated axons and associates with K⁺ channels. *Neuron* 24, 1037–1047.
- Prange, O., Wong, T.P., Gerrow, K., Wang, Y.T., and El-Husseini, A. (2004). A balance between excitatory and inhibitory synapses is controlled by PSD-95 and neuroligin. *Proc. Natl. Acad. Sci. USA* 101, 13915–13920.
- Prokop, A., and Meinertzhagen, I.A. (2006). Development and structure of synaptic contacts in *Drosophila*. *Semin. Cell Dev. Biol.* 17, 20–30.
- Roos, J., and Kelly, R.B. (1999). The endocytic machinery in nerve terminals surrounds sites of exocytosis. *Curr. Biol.* 9, 1411–1414.
- Roos, J., Hummel, T., Ng, N., Klambt, C., and Davis, G.W. (2000). *Drosophila* Futsch regulates synaptic microtubule organization and is necessary for synaptic growth. *Neuron* 26, 371–382.
- Rowen, L., Young, J., Birditt, B., Kaur, A., Madan, A., Philipps, D.L., Qin, S., Minx, P., Wilson, R.K., Hood, L., and Graveley, B.R. (2002). Analysis of the human neurexin genes: alternative splicing and the generation of protein diversity. *Genomics* 79, 587–597.
- Scheiffele, P. (2003). Cell-cell signaling during synapse formation in the CNS. *Annu. Rev. Neurosci.* 26, 485–508.
- Scheiffele, P., Fan, J., Choih, J., Fetter, R., and Serafini, T. (2000). Neuroligin expressed in nonneuronal cells triggers presynaptic development in contacting axons. *Cell* 101, 657–669.
- Shcherbata, H.R., Yatsenko, A.S., Patterson, L., Sood, V.D., Nudel, U., Yaffe, D., Baker, D., and Ruohola-Baker, H. (2007). Dissecting muscle and neuronal disorders in a *Drosophila* model of muscular dystrophy. *EMBO J.* 26, 481–493.
- Smith, L.A., Wang, X., Peixoto, A.A., Neumann, E.K., Hall, L.M., and Hall, J.C. (1996). A *Drosophila* calcium channel alpha1 subunit gene maps to a genetic locus associated with behavioral and visual defects. *J. Neurosci.* 16, 7868–7879.
- Sone, M., Suzuki, E., Hoshino, M., Hou, D., Kuromi, H., Fukata, M., Kuroda, S., Kaibuchi, K., Nabeshima, Y., and Hama, C. (2000). Synaptic development is controlled in the periaxonal zones of *Drosophila* synapses. *Development* 127, 4157–4168.
- Song, J.Y., Ichtchenko, K., Sudhof, T.C., and Brose, N. (1999). Neuroligin 1 is a postsynaptic cell-adhesion molecule of excitatory synapses. *Proc. Natl. Acad. Sci. USA* 96, 1100–1105.
- Stewart, B.A., Schuster, C.M., Goodman, C.S., and Atwood, H.L. (1996). Homeostasis of synaptic transmission in *Drosophila* with genetically altered nerve terminal morphology. *J. Neurosci.* 16, 3877–3886.
- Sugita, S., Saito, F., Tang, J., Satz, J., Campbell, K., and Sudhof, T.C. (2001). A stoichiometric complex of neurexins and dystroglycan in brain. *J. Cell Biol.* 154, 435–445.
- Tabuchi, K., and Sudhof, T.C. (2002). Structure and evolution of neurexin genes: insight into the mechanism of alternative splicing. *Genomics* 79, 849–859.
- Taniguchi, H., Gollan, L., Scholl, F.G., Mahadomrongkul, V., Dobler, E., Limthong, N., Peck, M., Aoki, C., and Scheiffele, P. (2007). Silencing of neuroligin function by postsynaptic neurexins. *J. Neurosci.* 27, 2815–2824.
- Thibault, S.T., Singer, M.A., Miyazaki, W.Y., Milash, B., Dompe, N.A., Singh, C.M., Buchholz, R., Demsky, M., Fawcett, R., Francis-Lang, H.L., et al. (2004). A complementary transposon tool kit for *Drosophila melanogaster* using P and piggyBac. *Nat. Genet.* 36, 283–287.
- Torroja, L., Packard, M., Gorczyca, M., White, K., and Budnik, V. (1999). The *Drosophila* beta-amyloid precursor protein homolog promotes synapse differentiation at the neuromuscular junction. *J. Neurosci.* 19, 7793–7803.
- Ushkaryov, Y.A., Petrenko, A.G., Geppert, M., and Sudhof, T.C. (1992). Neuexins: synaptic cell surface proteins related to the alpha-latrotoxin receptor and laminin. *Science* 257, 50–56.
- Wagh, D.A., Rasse, T.M., Asan, E., Hofbauer, A., Schwenkert, I., Durrbeck, H., Buchner, S., Dabauvalle, M.C., Schmidt, M., Qin, G., et al. (2006). Bruchpilot, a protein with homology to ELKS/CAST, is required for structural integrity and function of synaptic active zones in *Drosophila*. *Neuron* 49, 833–844.
- Yamagata, M., Sanes, J.R., and Weiner, J.A. (2003). Synaptic adhesion molecules. *Curr. Opin. Cell Biol.* 15, 621–632.
- Yoshihara, M., and Littleton, J.T. (2002). Synaptotagmin I functions as a calcium sensor to synchronize neurotransmitter release. *Neuron* 36, 897–908.
- Zeng, X., Sun, M., Liu, L., Chen, F., Wei, L., and Xie, W. (2007). Neuexin-1 is required for synapse formation and larvae associative learning in *Drosophila*. *FEBS Lett.* 581, 2509–2516.
- Zhang, W., Rohlmann, A., Sargsyan, V., Aramuni, G., Hammer, R.E., Sudhof, T.C., and Missler, M. (2005). Extracellular domains of alpha-neuexins participate in regulating synaptic transmission by selectively affecting N- and P/Q-type Ca²⁺ channels. *J. Neurosci.* 25, 4330–4342.